Experimental Investigation of the Flow Field Underneath a Generic High-Speed Train and the Effects of Ground and Train Roughness

Mattias Jönsson and Sigfried Loose

Abstract Results obtained from two component Particle Image Velocimetry (PIV) measurements on three different 1:50 generic high-speed train configurations hauled through a water towing tank over a smooth (Plexiglas) and a rough (grinding belt) ground at a speed of 4 m/s are presented. Principally, the three different generic high-speed train configurations are based on the same model (front car, two cars and tail car). The smooth generic high-speed train configuration (smooth GHSTC) reflects no bogies and covers the bogie cut outs and inter car gaps, the rough generic high-speed train configuration (rough GHSTC) is obtained by removing the bogies and leave the bogie cut outs and inter car gaps open and for the generic high-speed train configuration (GHSTC) the bogies are not removed but the inter car gaps are left open. A PIV set-up was chosen that the light sheet defines a vertical plane (XZ) between the ground and the train in the symmetry line of the train. Comparing the PIV results obtained for the GHSTC with full scale measurements, it was found that the same flow structures develop in the vicinity of the head and the tail of the train. But, the measured underfloor U-velocity of the downscaled model measurements did not reach the same value as those measured for the full scale high-speed train. The reason which is ascribed to the better aerodynamic underframe of the train model in the downscaled model measurements. The flow field underneath the GHSTC was fully developed at the beginning of the second car, in agreement to the full scale measurements. For the three train configurations three different flow fields underneath the train were obtained. The lowest velocities were found for the smooth GHSTC and the highest for the rough GHSTC. Further, the ground roughness changed the flow fields underneath the different train configurations.

M. Jönsson (✉) · S. Loose
German Aerospace Center, Bunsenstraße 10, 37073 Göttingen, Germany
e-mail: Mattias.Joensson@dlr.de

S. Loose
e-mail: Sigfried.Loose@dlr.de

A. Dillmann and A. Orellano (eds.), *The Aerodynamics of Heavy Vehicles III*,
Lecture Notes in Applied and Computational Mechanics 79,
DOI 10.1007/978-3-319-20122-1_2

1 Introduction

Ballast projection which is also known as ballast flight takes place whenever one or more stones start to move or fly underneath the train. The flying stones can damage the underframe equipment of the train. They can also damage trackside objects when the ballasts are reflected to the side. Ballast projection has been considered as a problem in train aerodynamics since the 1980s. Back then it was correlated with snow and ice accumulation on the train underframe and it's dropping during travel. This problem could be minimized e.g. by lowering the ballast [9]. Since the beginning of the 21st century ballast projection incidents were reported also in the absence of winter conditions [1]. This indicated that the aerodynamic loads induced by high-speed trains are high enough to move the ballasts on the track bed [7]. To gain more knowledge regarding this observation many interesting studies were made within the DeuFraKo project [5], which included a full scale measurement [2]. The full scale measurement techniques used have been installed in the track bed. They have to be below Top Of Rail (TOR) for security reasons. Therefore it was only possible to measure aerodynamic loads and the flow field between the ground and TOR. To investigate the entire gap between the ground and the train, two component Particle Image Velocimetry (PIV) [4] was conducted in the water towing tank at DLR Göttingen. The obtained results are discussed below.

2 Experimental Setup

2.1 Water Towing Tank Göttingen

The PIV measurements which are presented in this paper were all conducted in the water towing tank at DLR Göttingen. The water towing tank is 18 m long open steel tank with a cross-section of 1.1×1.1 m equipped with thick glass windows allowing the use of optical measurement techniques and flow visualization, see Fig. 1. The moving model rig is hauled with the help of a steel cable and an electrical motor (installed outside the tank) and travels on two rails installed on the upper edges of the tank. For the presented results a rig speed of 4 m/s was used, which corresponds to a Reynolds number of approximately 0.24 Mio based on the reference length of 0.06 m of the model and the kinematic viscosity of water [6]. The 1:50 train model configuration (front car, two cars and tail car) is mounted on the moving model rig with the help of eight NACA profiles, i.e. two NACA profiles per car. The NACA profiles press the train model into the water. The NACA profiles were chosen in a way that they minimize the influence of the mounting on the flow field. They were mounted on the roof to avoid disturbing the flow field underneath the train model. The effects of the NACA profiles on the flow field underneath the train model can not completely be neglected but they are considered as very small. For the correct train ground simulation a ground plate was installed into the tank. The ground plate

Fig. 1 A train model mounted on the moving model rig with the installed ground plate in the water towing tank at DLR Göttingen

was held by eight threaded rods allowing to adjust the ground clearance to any desired value. For this measurements a ground clearance between the wheel and the ground of 0.047 mm (235 mm in full scale) was chosen according to the standard ground clearance used in cross-wind measurements [6]. The ground plate consists of Plexiglas plates mounted on an aluminum frame. The plates had to be transparent for the laser light sheet needed for the PIV.

2.2 PIV Setup and Measurement for the Water Towing Tank

The sketch in Fig. 2 shows the two component PIV set-up used for the measurements in the water towing tank. The laser, laser light sheet optics, light sheet mirror and

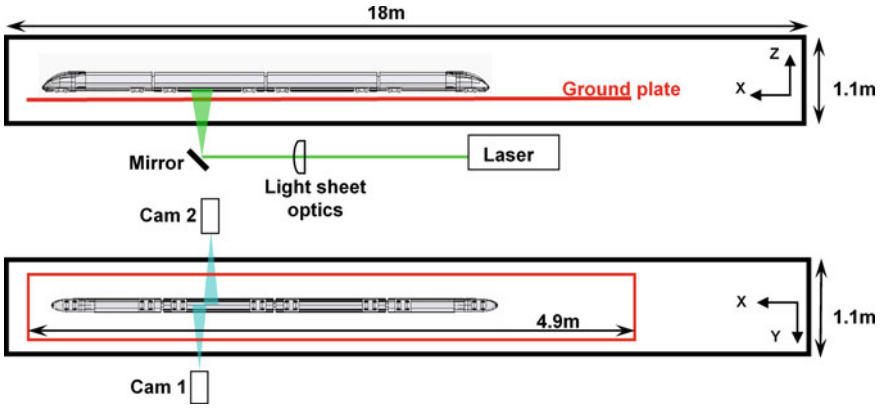

Fig. 2 Sketch of the two component PIV set-up for the water towing tank

cameras were all installed outside the water towing tank. The laser light sheet was arranged in a way that the vertical plane (XZ) between the ground and the train, at the centre line of the train, could be measured. This plane was chosen because the horizontal velocity underneath a train is expected to have their highest values in the centre line of the train [7]. The two cameras were installed perpendicular to the laser light sheet at both sides of the water towing tank. Two cameras were installed to increase the measurement field (also known as field of view). The complete field of view covered 0.065×0.025 m (W $\times$ H). Two PCO 1600 digital cooled 14 bit CCD cameras with a resolution of 1600×1200 pixels (W $\times$ H) were used, so that 450 pixels resolved the gap between the ground and the train. The PIV system had a maximum acquisition rate of 10 Hz. For the considered rig speed of 4 m/s it was possible to sample 5–6 PIV images per run. With a total field of view of 0.065×0.025 m (W $\times$ H) and a distance of 0.4 m between the images, the position had to be shifted 8 times to cover the entire train length ($\sim$2.1 m). At every position 10 runs were recorded and ensemble averaged to determine the mean flow field underneath the train. Additionally for a specific position 80 runs were recorded to be able to analyze the statistical convergence.

2.3 Train Model and Train Model Configurations

The used train model for the PIV measurements was a 4 unit (front car, 2 cars and tail car) 1:50 generic high-speed train model configuration. It is not possible to use more than 4 units owing to the dimensions of the water towing tank. The generic high-speed train model is a combination of the German high-speed train Inter City Express 3 (ICE3) and the Aerodynamic Train Model (ATM) which is similar to the ICE2. In Fig. 3 a close up view of the front is shown. The front of the train model has the shape of an ICE3 and shortly after the first bogie the cross-section smoothly changes to the cross-section of an ATM. A similar transition existed for the tail car since the ATM cross-section smoothly changes back to an ICE3 just in front of the last bogie. For the underframe itself the transition from an ICE3 to an ATM is difficult to detect. The most obvious between these two cross-sections is the two roof radiuses. But the influence between these two cross-sections on the underfloor aerodynamics is insignificant. Further, simplifications had to be realized for the downscaled model geometry. They are visible at the bogies where a lot of details were neglected.

Three different train configurations were realized by manipulating the underframe on the same train model. The configurations are characterized by different degrees

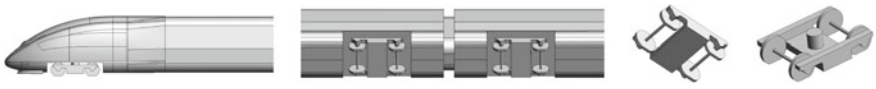

Fig. 3 The 1:50 generic high-speed train model: Front, underbelly and simplified bogie

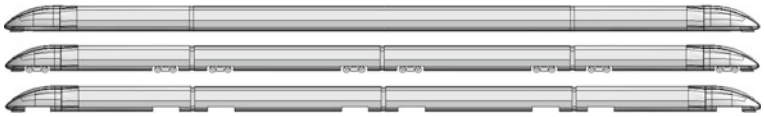

Fig. 4 The three train configurations: The smooth GHSTC (*upper*), the GHSTC (*middle*) and the rough GHSTC (*lower*)

of roughness. The generic high-speed train configuration (GHSTC) is a conventional high-speed train with inter car gaps and two bogies per car. For the smooth generic high-speed train configuration (smooth GHSTC) the bogies were removed and the bogie cut outs and the inter car gaps were covered. Hence a completely smooth underframe without protruding objects or gaps was realized. For the third configuration i.e. the rough generic high-speed train configuration (rough GHSTC), the bogies were removed and the bogie cut outs and inter car gaps were left open. CAD models of the three train configurations are presented in Fig. 4.

2.4 Ground Configurations

Each of the three different train configurations were all measured with the smooth and the rough ground. Thus in total six test cases were investigated. The smooth ground was realized with a smooth Plexiglas plate. For the rough ground additional Plexiglas plates were mounted on the ground plate and a grinding belt was glued on these additional plates. For the PIV measurements a small part of the grinding belt was removed, to guarantee optical accessibility for the laser light sheet, see Fig. 5. The roughness of the grinding belt was chosen such that the grain size corresponds to a 1:50 ballast stone. According to the European standard [3] the ballast stones selected for track beds are limited by holes of sieves with a width of 22.4–63 mm. This allows stones of sizes between 31.5 and 50 mm or 31.6 and 63 mm. The applied grinding belt had a grain size of less than 0.764 mm. No rails were mounted on both

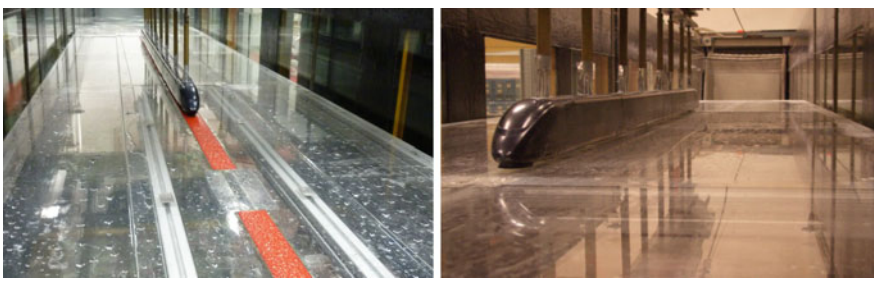

Fig. 5 The two ground configurations, rough ground (*left*) and smooth ground (*right*)

ground configurations to guarantee the optical access for the cameras. The influence of the rails is therefore not considered. But this simplification is not severe since the effect of the rails on the flow field in the center line of the train is rather small.

3 Data Evaluation

The major steps in the evaluation of the PIV data are listed and described below.

(1) Calculate the flow field with the help of the cross-correlation technique [8] between the PIV images.
(2) Find the shift between the runs to allocate the exact position of the train.
(3) Shift the data into its right position and average the overlap between the cameras.
(4) Interpolate the data on a global grid for the calculation of the ensemble average and the standard deviation, as in Eqs. 1 and 2.
(5) Use the ensemble average flow field at every position to construct the entire flow field underneath the train.

$$C(x_j, z_k) = \frac{1}{n} \sum_{i=1}^{n} C_i(x_j, z_k) \tag{1}$$

$$C_{STD}(x_j, z_k) = \sqrt{\frac{1}{n-1} \sum_{i=1}^{n} (C_i(x_j, z_k) - \overline{C}(x_j, z_k))^2} \tag{2}$$

For the cross-correlation of the PIV images a multigrid interrogation (grid refinement) was used with a final interrogation size of 24×24 pixels (0.522×0.522 mm) with an overlap of 75 %. With this configuration the gap between the ground and the train was resolved with 75 data points.

The shift between the runs was calculated to enhance the accuracy of the ensemble average. Reference lines were painted on the side of the train to identify the shift in the middle of a car or for the smooth GHSTC. For the later no characteristics such as the bogies of the train existed.

The velocity field from both cameras was then shifted into its right position and the overlap between the cameras averaged. With the data at its right position the data could be interpolated on a new global equidistant grid ($\Delta x = 0.13$ mm, $\Delta z = 0.13$ mm) for statistical averaging. The outer edges of the mean flow field were obtained with a lower sample rate due to the shift between the runs. Therefore data points generated in less than 8 runs (out of total of 10 runs) were excluded. For the measurements for which the position was fixed and than around 80 runs were realized the data fields of all of the realized runs were averaged. The last step was to shift the ensemble averages into the correct positions underneath the train and to average the overlaps between the different positions. With this principle the flow field underneath the entire train was reconstructed.

4 Results

4.1 Velocities Along the Train Length

The mean flow field underneath the train can be divided into the three regions, the flow around the head, along the train body and around the tail. This can be seen in Fig. 6, where the normalized horizontal component U of the mean velocity field is plotted along the length of the train for the three considered trains and both ground types. The flow field in the region close to the head and before the first train axle, reflects a positive U-velocity maximum which is followed by a negative U-velocity minimum which is the head effect. In front of the head the flow is pushed in the traveling direction of the train. Close to the head displacement causes the flow to draw aside in perpendicular to the traveling direction. The result is a reversed flow region directly underneath the head (the negative U-velocity minimum). Further downstream the train drags fluid in traveling direction. Thus the U-velocity is increasing with the train length until the 2nd car is reached. There the U-velocity settles around a constant value. The flow field changes then at the tail of the train (at the last bogie) where the third and last region is observed. Part of the third region is the near wake, reflected

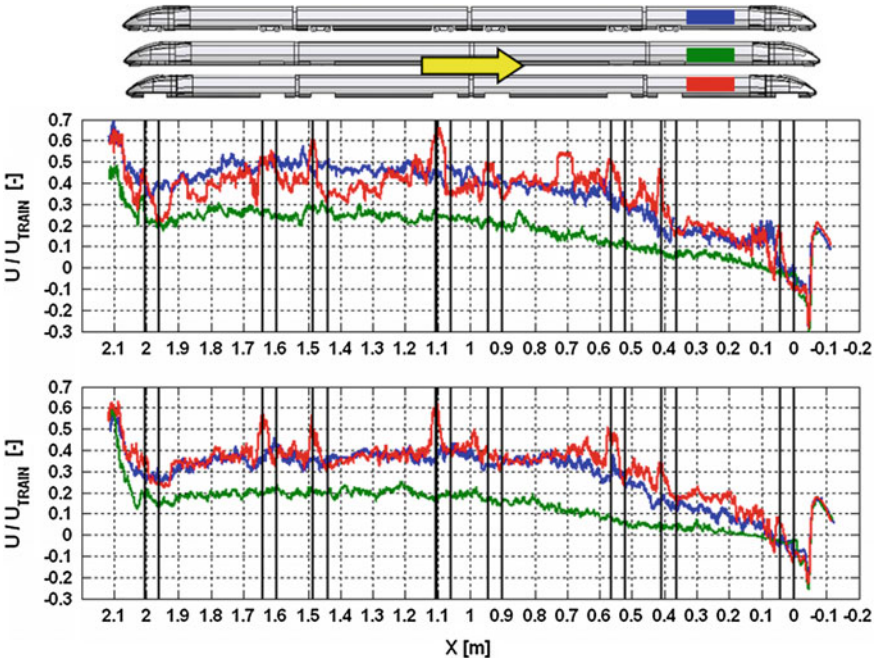

Fig. 6 Normalized U-velocity at TOR ($Z/H_{GAP} = 0.4753$) along the train length for the GHSTC (*blue*), the smooth GHSTC (*green*) and the rough GHSTC (*red*) for the smooth (*upper plot*) and the rough (*lower plot*) ground. The *black vertical lines* are the positions of the train axles

by a tiny decrease of the U-velocity just before the tail and directly after a strong acceleration of the flow. The smooth GHSTC shows the lowest U-velocity for both ground types. This is not surprising since this configuration has a smooth underframe with no protruding objects. The behavior for the GHSTC and the rough GHSTC is different due to ground roughness. For the rough ground the rough GHSTC produces a higher U-velocity at the front car than for the GHSTC. Thereafter the distribution of the U-velocity of both train configurations is almost similar. Only in the vicinity of the bogies the rough GHSTC produces higher U-velocity than the GHSTC. However for the smooth ground the U-velocities obtained for the GHSTC and the rough GHSTC are the same at the front car and the 1st car. For the second half of the train the U-velocity obtained for the rough GHSTC are lower than those measured for the GHSTC. Also for the smooth ground higher U-velocity values are observed around the bogies for the rough GHSTC. The effect of the ground roughness on the velocity distribution over the gap between the ground and the train is discussed more in detail in Sect. 4.2.

In Fig. 7 the normalized vertical component W of the mean velocity field is plotted along the train length for the three train configurations and both ground types. As expected the vertical velocity values for the smooth GHSTC are small except around the head and the tail due to the absence of protruding objects. The small

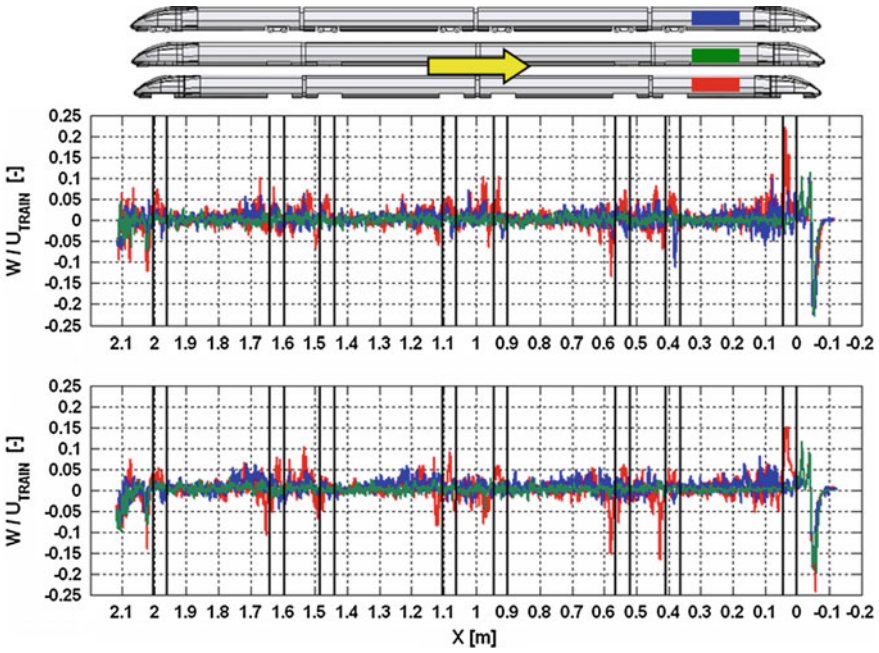

Fig. 7 Normalized W-velocity at TOR ($Z/H_{GAP} = 0.4753$) along the train length for the GHSTC (*blue*), the smooth GHSTC (*green*) and the rough GHSTC (*red*) for the smooth (*upper plot*) and the rough (*lower plot*) ground. The *black vertical lines* are the positions of the train axles

W-velocity fluctuations around zero are considered to be noise. For the two other train configurations the effects of the bogies and the open bogie cut outs are reflected in the W-velocity. The highest W-velocities in both directions are found for the rough GHSTC. The effects from the bogie areas are stronger at the beginning of the train than at the end. This is due to the boundary layer growth underneath the train. A maximum W-velocity value with a direction towards the ground are observed at every bogie followed by a W-velocity variations around zero which settles itself around the middle of every car. For the open bogie cut outs a maximum in the W-velocity towards the train appears first as the flow approaches the bogie cut out. Then a strong maximum of the W-velocity with a direction towards the ground appears where the flow leaves the bogie cut out. This is also followed by W-velocity variations with amplitudes which decrease in the middle of the car. The GHSTC and the rough GHSTC produce the same W-velocity value as the smooth GHSTC at the middle of the car, for every car, and the W-velocity stay constant until the next downstream bogie. This is interpreted as a W-velocity for the GHSTC and the rough GHSTC which is zero at this position just as that obtained for the smooth GHSTC.

4.2 Velocity Profiles

To obtain a better overview of the development of the flow field behavior, additionally velocity profiles over the gap between the ground and the train were extracted. The velocity profiles shown are from the measurements for a selected position and statistical averaging from 80 runs, instead of the 10 runs used for the results along the train length. In Fig. 8 the three train configurations are compared with each other for five different positions underneath the train. The positions underneath the train are indicated by the red vertical lines on the train configurations above the velocity profile plots. The front car velocity profile is the plot to the right and the tail car velocity profile is the plot to the left. The U-velocity is normalized with the train speed and plotted against the height normalized with the gap distance between the ground and the train underbelly. The ground is at $Z/H_{GAP} = 0$ where $U/U_{TRAIN} = 0$ and the train underbelly is at $Z/H_{GAP} = 1$ where $U/U_{TRAIN} = 1$.

Studying the velocity profiles from the right to the left plot the flow field development underneath the train is analyzed. The flow develops along the entire gap, especially at the ground, until it reaches the 2nd car where the flow is fully developed. Comparing the last two velocity profiles (two velocity profiles to the left) no difference can be observed, hence the flow is fully developed. The smooth GHSTC produces the lowest U-velocity over the entire gap for both ground types. Comparing the results for GHSTC and the rough GHSTC in Fig. 8 it can be seen that the flow of the two train configurations develops differently for the two ground types. The first three velocity profiles (front car, downstream of the 3rd and 4th bogie) of the GHSTC and the rough GHSTC are nearly the same for both ground types. Differences are observed at the end of the 2nd car and later at the tail car. For the rough ground the

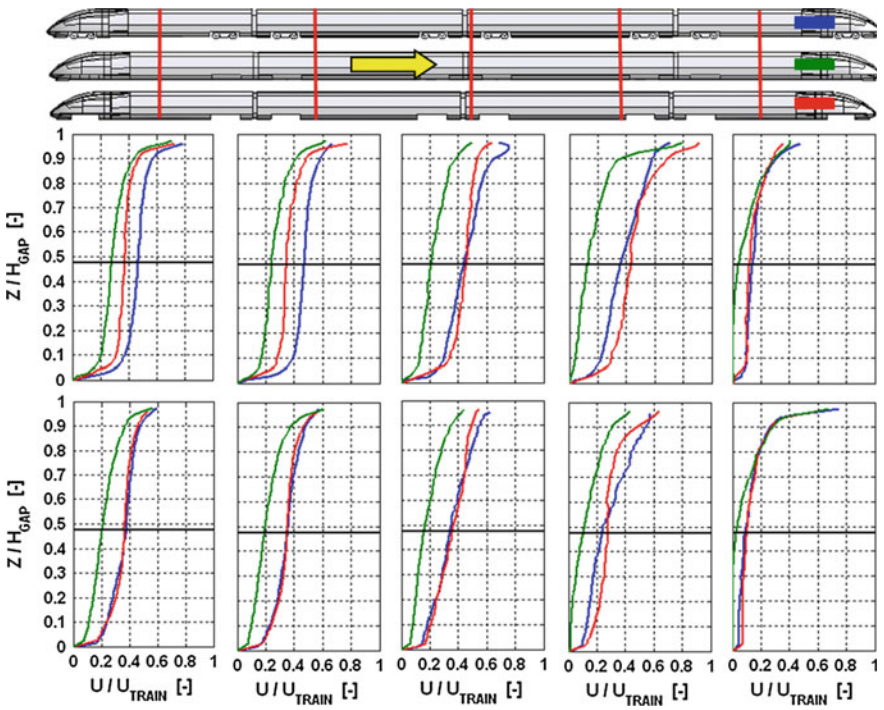

Fig. 8 Velocity profiles over the gap between the ground and the train underframe for the GHSTC (*blue*), the smooth GHSTC (*green*) and the rough GHSTC (*red*) for the smooth (*upper row*) and the rough (*lower row*) ground. The *red vertical lines* on the train configurations indicate the velocity profile positions and the *black horizontal line* is the TOR

velocity profiles are similar. But for the smooth ground the velocities of GHSTC overtake those of the rough GHSTC finally leading to higher U-velocity values.

Regarding ballast projection the velocity below TOR and the velocity gradient at the ground are two important factors among others. The velocity gradient at the ground is proportional to the shear force on the ground i.e. the ballasts. If ballast starts to move or elevates the velocity close to the ground has a big impact on the forces on the moving or flying ballast. Ranking the train configurations regarding the risk for ballast projection, by looking at the mean U-velocity component, the smooth GHSTC would be less sensible than the two other train configurations. The reason is that it has the lowest U-velocity and also the lowest velocity gradient close to the ground for both ground types. The ranking of the most susceptible train configuration is more difficult to develop due to the ground roughness effect between the GHSTC and the rough GHSTC. For the rough ground the rough GHSTC is the most susceptible due to the higher U-velocities around the bogies. However for the smooth ground it is believed that ballast projection is more an issue for the GHSTC. The rough GHSTC generates higher U-velocity values in the vicinity of the bogies but the U-velocity

values between the bogies for the 2nd car and the tail car are lower. The difference between the velocity profiles measured for the GHSTC and the rough GHSTC for the 2nd car and the tail car is larger than the difference of the velocity profiles behind the fourth bogie. Therefore the GHSTC on the smooth ground is considered to be more susceptible for ballast projection.

All velocity profiles obtained for the 1st car and the tail car are plotted in Fig. 9. The effect of the ground roughness can be extracted by comparing the velocity profiles of the smooth ground (full lines) with the velocity profiles of the rough ground (dashed lines). For the smooth GHSTC the difference between the smooth and the rough ground types increases along the train length as the boundary layers develops. The ground roughness slows down the flow in the traveling direction underneath the train and with increasing U-velocities the difference is also increasing between the results of the ground types. The increasing difference between the ground configurations along the train length could not be identified for the GHSTC, where a clear difference was found from the beginning until the end of the train. For the GHSTC and the smooth GHSTC a difference of the flows for the two ground types was found over the entire gap. This was only observed for the front car and around the bogies for the rough GHSTC, see the plot to the right in Fig. 9. Further downstream the train the difference could only be found below TOR. The train roughness of the rough GHSTC is large enough that the ground roughness only influences the flow field close to the ground and not the flow field close to the train. The GHSTC is more sensitive to the ground roughness than the rough GHSTC, or the GHSTC is not as rough as the rough GHSTC.

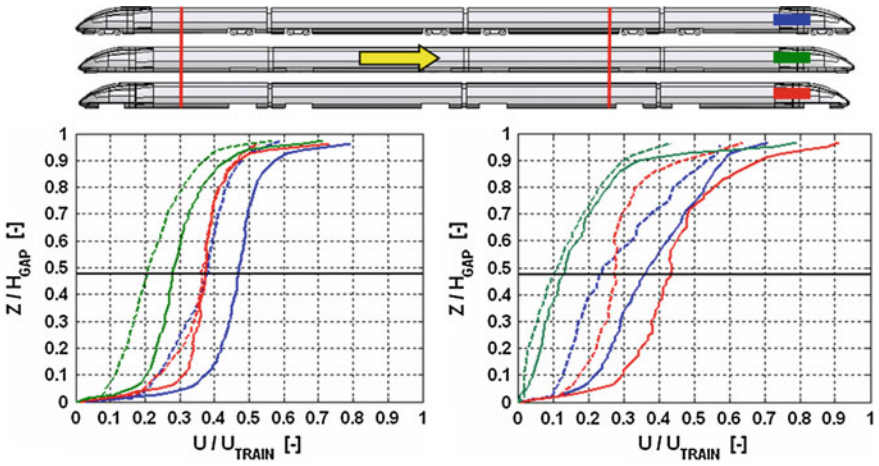

Fig. 9 Velocity profiles after the 3rd bogie and in the *middle* of the tail car for the GHSTC (*blue*), the smooth GHSTC (*green*) and the rough GHSTC (*red*) for the smooth (*full lines*) and the rough (*dashed lines*) ground. The *red vertical lines* on the train configurations indicate the velocity profile positions and the *black horizontal line* is the TOR

4.3 Standard Deviation Profiles

Profiles of the standard deviation of the U-velocity (U_{STD}) over the gap between the ground and the train underframe are plotted in Fig. 10 for the smooth (upper row) and for the rough (lower row) ground type. Comparing the three train configurations for both ground types it is easy to observe that the rough GHSTC leads to the highest U_{STD} values for all positions. This train configuration is also the roughest one and therefore it should lead to higher U_{STD} values. The lowest U_{STD} values was reached by the smooth GHSTC, this was also expected due to the completely smooth underframe. The value of the U_{STD} for the smooth GHSTC lies around 0.05–0.06 for the region above TOR at the beginning of the train and with the train length the U_{STD} value below TOR develops to a constant value over the gap of 0.05–0.06 for both ground types. The relation for the GHSTC to the other two train configurations changes with the train length. At the beginning of the train the behavior of the GHSTC is very close to that of the rough GHSTC and far away from the smooth GHSTC. For the next two downstream positions, i.e. downstream region of the 3rd and 4th bogie, the GHSTC profiles lies between those of the two other train configurations. This indicates that the open bogie cut outs are able to produce higher additional

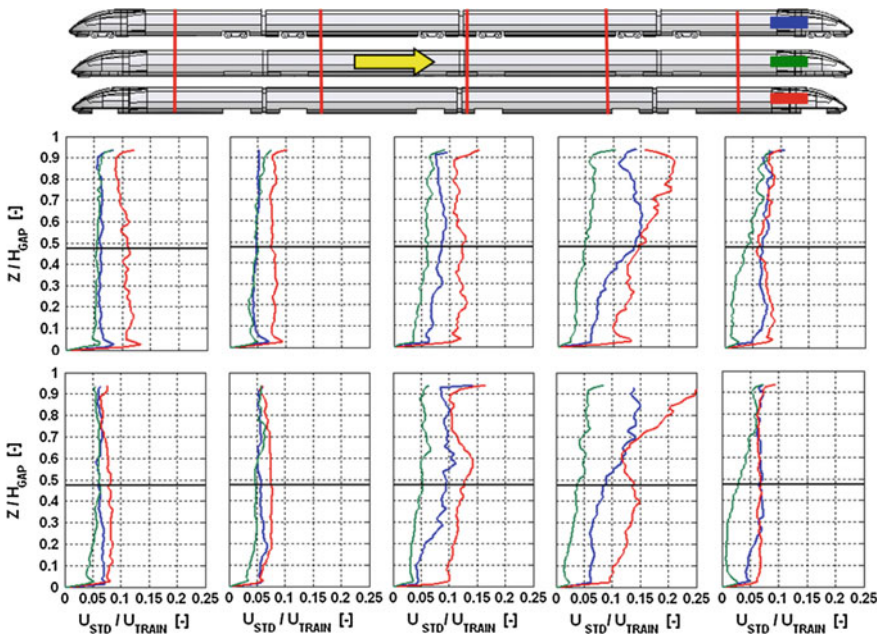

Fig. 10 U_{STD} profiles over the gap between the ground and the train underframe for the GHSTC (*blue*), the smooth GHSTC (*green*) and the rough GHSTC (*red*) for the smooth (*upper row*) and the rough (*lower row*) ground. The *red vertical lines* indicate the velocity profile positions and the *black horizontal line* is the TOR

ΔU-velocity to the mean than for the bogies and of course the smooth wall. For the two last positions the U_{STD} values of GHSTC are similar to the smooth GHSTC, except for the rough ground type where a difference was found in the region below TOR. The reason might be, that when the flow is fully developed the disturbances from the upstream bogie has a minor influence on the flow from the middle of the car until the next bogie. This is not the case for the rough GHSTC which produces a higher U_{STD} value, the disturbances from the open bogie cut out have not settled as for the GHSTC.

Summarizing the velocity profiles results in Sect. 4.2 and the results from the U_{STD} profiles the less sensible for ballast projection is the smooth GHSTC for both ground types. The smooth GHSTC are characterized by the lowest value of both quantities. For the ballast projection ranking of the train configurations the Gaussian distribution (or normal distribution) was assumed for the velocity distribution underneath the train. Applying the 2σ rule, that 95 % of all values extracted from the normal distribution are within 2σ of the average (in this case 2 U_{STD} of the mean U-velocity). Ranking the train configurations after the upper limit of the U-velocity distribution the rough GHSTC is the most susceptible for ballast projection on both ground types. The rough GHSTC reflects the highest U-velocity for all five positions for the rough ground. For the smooth ground the rough GHSTC leads to the highest U-velocity values for the front car and after the 3rd and 4th bogie. However at the end of the 2nd car the GHSTC produces a larger U-velocity values and for the tail car the GHSTC and the rough GHSTC had the same U-velocity. The U-velocity of the GHSTC was only higher at one position underneath the train and therefore the rough GHSTC was considered to be more susceptible for ballast projection.

The ground roughness also had an effect on the U_{STD} values. In Fig. 11 the U_{STD} profiles are plotted for both ground types for three different positions underneath the train. The ground roughness effect differs for the three train configurations. For the smooth GHSTC a small difference between the ground types was found for the

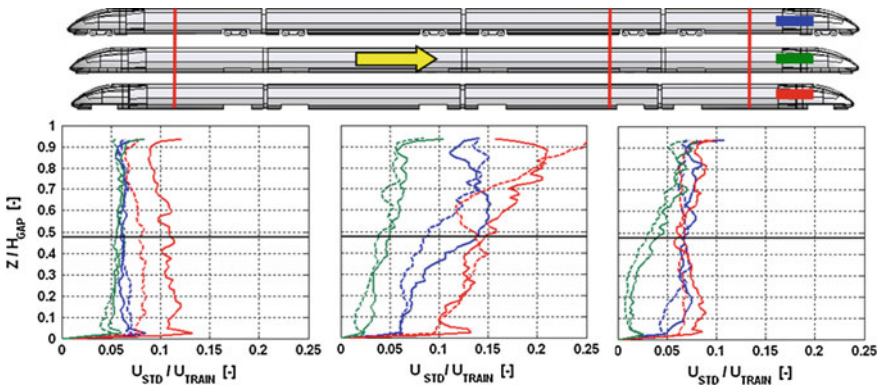

Fig. 11 U_{STD} profiles for the GHSTC (*blue*), the smooth GHSTC (*green*) and the rough GHSTC (*red*) for the smooth (*full lines*) and the rough ground (*dashed lines*). The *red vertical lines* indicate the velocity profile positions and the *black horizontal line* is the TOR

first half of the train where the smooth ground leads to a higher U_{STD} value. For the second half of the train the difference decreases and it's hard to differentiate the results obtained for the two ground types. The GHSTC showed the same ground roughness effect like the smooth GHSTC for the first half of the train. For the second half of the train the relation between the ground types changed and the rough ground generates a higher U_{STD} value than the smooth ground. The tendency for the ground roughness effect is different for the rough GHSTC than for the two other train configurations. The difference between the ground types increases with the train length. The U_{STD} value measured for the smooth ground was a bit higher than those for the rough ground measurements of the front car. Around the bogies the ground types showed little influence and a clear difference at the end of the train where the smooth ground lead to higher U_{STD} values than for the rough ground.

4.4 Comparison with Full Scale Measurements

The PIV results from the water towing tank were also compared to full scale measurements [2] to identify differences and similarities between full scale and downscaled model measurements. For the comparison the length of the train model was multiplied with the model scale factor. Two comparisons were conducted due to the different lengths of the train sets (14 units for the full scale and 4 units for the downscaled model measurements), one where the first axle and one where the last axle of the trains were aligned, see Fig. 12. The two curves do not fit perfectly, due to the

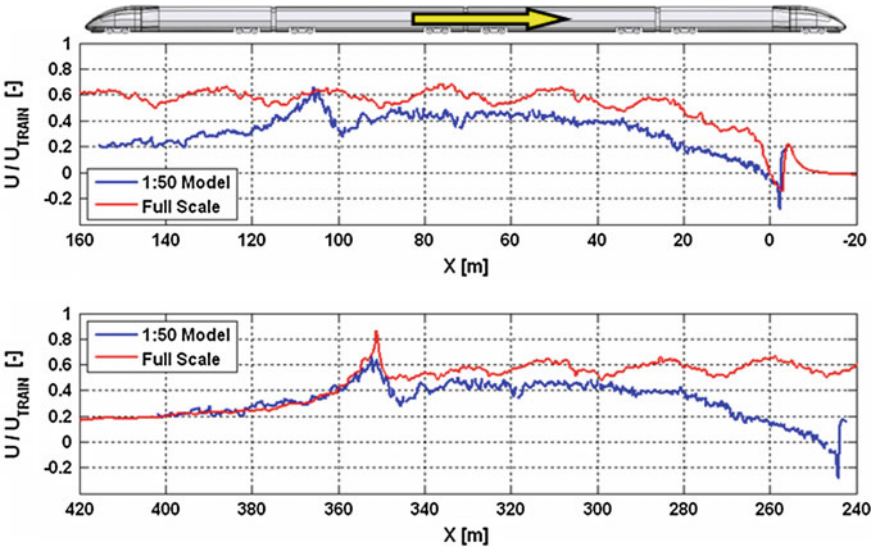

Fig. 12 Comparison to full scale measurements. In the *upper plot* the first axles of the trains are aligned and in the *lower plot* the last axle of the trains are aligned

different geometrical shapes of the trains. For the downscaled model measurements a generic high-speed train configuration was used and for the full scale measurements the Italian high-speed train ETR 500 was measured. However the same flow field characteristics were found around the head and the tail of the train. The flow field was also fully developed at the beginning of the 2nd car, which was also observed for the full scale measurements. The U-velocity distribution obtained for the downscaled model measurements is always lower than that of the full scale measurements. The reason is that the train model in the downscaled model measurements is aerodynamically better than the ETR 500. The simplified bogies, in Fig. 3, used for the water towing tank are completely smooth on the surface facing the ground. This is not the case for a full scale bogie on a train where a lot of protruding objects exists such as gearboxes, electrical motors, cables etc. There are also a lot of cavities where the air can flow into and be accelerated by the train, the simplified bogies shields the bogie cut out and makes the train underframe smoother than for the ETR 500. The bogie differences is also one of the reasons that the downscaled model measurements does not have a self-similar or wave pattern which was found for the full scale measurements. Another reason is that for a full scale train there are also air outlets (cooling air) on the underframe of the train which gives a momentum into the flow field. The comparison showed that the normalized U-velocity distribution underneath the train for the downscaled model measurements is comparable to that of a full scale high-speed train cruising at a speed of 250 km/h.

5 Conclusions

- It was possible to create three different flow fields underneath the train by manipulating the underframe on the same train model.
- The flow fields were fully developed at the beginning 2nd car. This was also observed for the full scale measurements.
- Considering the different train geometries and the simplifications that were done for the downscaled model measurements a comparable U-velocity distribution to the full scale measurements was achieved.
- The ground roughness changed the flow fields underneath all three train configurations.
- The smooth GHSTC is considered to be the less sensitive and the rough GHSTC the most susceptible for ballast projection.
- Important information can be extracted from downscaled model measurements, however to extrapolate the results into full scale should be done with caution.

References

1. Claus, P.: WP 1.2 ballast projection: prestudy of ballast projection incidents. In: DeuFraKo Project Aerodynamics in Open Air (AOA) (2007)
2. Deeg, P., Jönsson, M., Kaltenbach, H.J., Schober, M., Weise, M.: Cross-comparison of measurement techniques for the determination of train induced aerodynamic loads on the trackbed. In: Proceedings of the BBAA VI, Milano, Italy, 20–24 July 2008. http://bbaa6.mecc.polimi.it/uploads/treni/BPR04.pdf
3. Din, E.N.: 13450:2002: Aggregates for Railway Ballast. Gesteinskörnung für Gleisschotter, Deutsche Fassung (2002)
4. Eckelmann, H.: Einführung in die Strömungsmeßtechnik. B.G Teubner, Stuttgart (1997)
5. Kaltenbach, H.J.: WP1 underfloor aerodynamics summary report. In: DeuFraKo Project Aerodynamics in Open Air (AOA) (2008)
6. prEN 14067–6:2006: Railway Applications—Aerodynamics—Part 6: Requirements and Test Procedures for Cross Wind Assessment (2006)
7. Quinn, A.D., Hayward, M., Baker, C.J., Schmid, F., Priest, J.A., Powrie, W.: A full-scale experimental and modelling study of ballast flight under high-speed trains. In: Rai, F-J. (ed.) Proceedings of Institute of Mechanical Engineering (2009). doi: 10.1243/09544097JRRT294
8. Raffel, M., Willert, C.E., Wereley, S.T., Kompenhans, J.: Particle Image Velocimetry, 2nd edn. Springer, Berlin (2007)
9. Shinojima, K.: Study on the phenomena of snow adhering to and dropping from shinkansen train, and the countermeasures. Q. Rep. **25**(2), 41–44 (1984)

Springer

http://www.springer.com/978-3-319-20121-4

The Aerodynamics of Heavy Vehicles III
Trucks, Buses and Trains
Dillmann, A.; Orellano, A. (Eds.)
2016, IX, 428 p., Hardcover
ISBN: 978-3-319-20121-4